Research in Astronomy and Astrophysics, 23:035016 (12pp), 2023 March https://doi.org/10.1088/1674-4527/acb9df

Six Newly Discovered Eclipsing Binary Systems in the TESS field

Burak Ulaş and Vildan Ayan
Department of Space Sciences and Technologies, Faculty of Sciences, Çanakkale Onsekiz Mart University, Terzioğlu Campus, TR 17100, Çanakkale, Turkey; burak.ulas@comu.edu.tr
Received 2022 December 25; revised 2023 January 30; accepted 2023 February 1; published 2023 March 10

Abstract

We present the first detailed investigation of six eclipsing binary systems in the TESS field. The TESS light curves of the targets are analyzed by determining the initial effective temperatures via SED fits. The absolute parameters are derived and the systems are compared to well-known binaries of the same type. Results show that CD-58791, CD-621257 and TYC 9356-355-1 are detached binary systems. CD-54942 and UCAC4 136-007295 are contact binaries while TYC 8508-1413-1 is a semidetached system.

Key words: (stars:) binaries: eclipsing – stars: fundamental parameters – stars: individual (CD-54 942, CD-58 791, CD-62 1257, TYC 8508-1413-1, TYC 9356-355-1 and UCAC4 136-007295)

1. Introduction

Studies on eclipsing binary systems improved our understanding of the structure and evolution of stars in various circumstances. Since the observation of Mizar, more than four hundred years of effort put forth by researchers to observe, discover, classify and reveal the characteristics of binary systems resulted in an ability to determine the light and absolute parameters, thus, making incisive estimations on their structural properties and evolutional paths. Being powerful tools for deriving the crucial properties of the stars, binary star systems still hold their solid ground as one of the leading research topics in stellar astrophysics.

Space observations are a milestone in finding a chance to look at the binary stars in a different way. They allow us to determine the variations with small amplitudes and discover very faint binaries that can be improbable to detect with numerous ground-based instruments. The discoveries made by using the data from Kepler (Borucki et al. 2010) and Transiting Exoplanet Survey Satellite (TESS, Ricker et al. 2015) missions played an important role in improving our knowledge of various types of stars, as well as binary systems. They also provided a dramatic increment in the number of known systems. As of the moment, Kepler Eclipsing Binary Catalog of Kirk et al. (2016) contains 2920 systems while Prša et al. (2022) cataloged 4584 binaries in their TESS Eclipsing Binary catalog.

The systems investigated in this paper were first validated as eclipsing binaries in the eclipsing binary catalog of Prša et al. (2022) where the authors classified the targets based on their TESS light curves. The targets were also cataloged by the Gaia data releases (Gaia Collaboration et al. 2016, 2018, 2022). CD-54942, CD-58791 and TYC 9356-355-1 also appeared in the releases of the Radial Velocity Experiment (RAVE) (Kordopatis et al. 2013; Kunder et al. 2017; Steinmetz et al. 2020). Sharma et al. (2018) listed UCAC4 136-007295 in their High Efficiency and Resolution Multi-Element Spectrograph (HERMES) catalog.

The lack of detailed information on the systems in the literature motivated us to study them in detail. Our study is the first one that focuses on the analyses of the light curves and the determination of binary parameters. The next section gives the details of the data used in the study while Section 3 deals with the derivation of the initial effective temperatures, calculation of the orbital periods and the analyses of the light curves. In the last section, we conclude the results and compare the systems with well-known binaries with the same morphologies.

2. Light Curves

We collected the TESS light curve data on the systems via the Mikulski Archive for Space Telescopes (MAST) portal.[1] The magnitude values were derived following the TESS magnitudes (Stassun et al. 2019) and using the formula $-2.5 \log F$ where F is the Pre-search Data Conditioning Simple Aperture Photometry (PDC SAP) flux values stored in the data files. The data are from sectors 3, 4, 5 and 6 for CD-54942, sectors 2, 3 and 4 for CD-58791, sector 13 for CD-621257, sectors 3 and 4 for TYC 8508-1413-1, sectors 1 and 13 for TYC 9356-355-1, and sectors 9, 10 and 11 for UCAC4 136-007295. The TESS magnitudes are $10^{\rm m}.785$, $9^{\rm m}.718$, $9^{\rm m}.891$, $10^{\rm m}.787$, $10^{\rm m}.238$ and $12^{\rm m}.406$ for CD-54942, CD-58791, CD-621257, TYC 8508-1413-1, TYC 9356-355-1 and UCAC4 136-007295, respectively.

[1] mast.stsci.edu/portal/Mashup/Clients/Mast/Portal.html

Table 1
Calculated Times of Minimum Light for the Systems

System	BJD-2457000	Error	Min. type
CD-54942	1386.126517	0.000001	I
CD-54942	1385.971296	0.000001	II
CD-54942	1386.436137	0.000001	I
CD-54942	1386.281039	0.000001	II
CD-54942	1386.745805	0.000001	I
CD-54942	1386.590640	0.000001	II
⋮	⋮	⋮	⋮

Note. TYC 8508, TYC 9356 and UCAC4 136 refer to TYC 8508-1413-1, TYC 9356-355-1 and UCAC4 136-007295, respectively. This table is for guidance, and its full version is available in electronic form.

The one orbital period long light curves of the systems are depicted in Figure 1. As seen from the figure, the shapes of the curves resemble the typical variation of eclipsing binary systems in several morphologies. The depths of primary and secondary minimums are $0\overset{m}{.}31$ and $0\overset{m}{.}26$ for CD-54942, $0\overset{m}{.}283$ and $0\overset{m}{.}282$ for CD-58791, $0\overset{m}{.}24$ and $0\overset{m}{.}20$ for CD-621257, $0\overset{m}{.}42$ and $0\overset{m}{.}16$ for TYC 8508-1413-1, $0\overset{m}{.}40$ and $0\overset{m}{.}14$ for TYC 9356-355-1, and $0\overset{m}{.}22$ and $0\overset{m}{.}21$ for UCAC4 136-007295. The durations are $3\overset{h}{.}8$ and $3\overset{h}{.}4$, $5\overset{h}{.}5$ and $5\overset{h}{.}4$, $5\overset{h}{.}6$ and $5\overset{h}{.}3$, $2\overset{h}{.}9$ and $2\overset{h}{.}8$, $3\overset{h}{.}5$ and $3\overset{h}{.}8$, and $6\overset{h}{.}1$ and $5\overset{h}{.}9$ for the primary and secondary minimum of CD-54942, CD-58791, CD-621257, TYC 8508-1413-1, TYC 9356-355-1 and UCAC4 136-007295, respectively; 967 times of minimum light for the targets were also calculated from the TESS light curves using the method of Kwee & van Woerden (1956) and listed in Table 1.

3. Analyses of the Light Curves

The systems were recently classified as eclipsing binary candidates by Prša et al. (2022), however, their binary parameters were not determined in the literature. The lack of detailed information about the systems necessitates the derivation of some crucial parameters prior to the light curve analyses. We first determined the mass ratio for the systems via q-search procedure by using the 2015 version of the Wilson–Devinney code (Wilson & Devinney 1971; Wilson et al. 2020) on 1000 normalized data points of the light curves. A lack of morphological classes of the systems directed us to apply q-search in two different morphological assumptions for each system. The contact and semidetached approaches were used for CD-54942 and UCAC4 136-007295. The q-searches with the contact approach were applied in the range of $q = 0.0$–2.0 to avoid missing the more accurate values larger than 1.0. The process outputted unphysical results for the q values larger than 0.5 for CD-54942. The q-searches for CD-58791, CD-621257, TYC 8508-1413-1 and TYC 9356-355-1, on the other hand, were made in detached and semidetached mode. The results of the q-search are shown in Figure 2 which indicates that CD-54942 and UCAC4 136-007295 are probably contact binary systems whereas detached morphology is more accurate for CD-58791, CD-621257 and TYC 9356-355-1. TYC 8508-1413-1 is found to be a semidetached binary based on our q-search results. However, one must bear in mind that the light curve is not sensitive to mass ratio for detached binaries and semidetached systems that show partial eclipses (Terrell & Wilson 2005), therefore, some further properties must be taken into account to decide the morphology as we remark in corresponding subsections.

The effective temperature also significantly impacts deriving physically meaningful results by light curve analysis. The systems were not studied in detail previously, thus, we faced the lack of reliable effective temperature values for the components in the literature as expected. We constructed spectral energy distributions (SEDs) through Virtual Observatory SED Analyzer (VOSA, Bayo et al. 2008) using the photometric data given by the VizieR database (Ochsenbein et al. 2000) to derive the temperatures for the components of the systems. During the SED analysis, the data were fitted using a chi-squared fit or binary fit (two component approach) with a parameter-grid search to obtain the optimized Kurucz atmosphere model (Kurucz 1979). The search domain for the temperatures was set between 3500 and 10,000 K while the interval for log g values, which has a minor effect on SED, was between 2.5 and 5.0. A good fit corresponds to the V_{gfb} value, a value for estimating the goodness of fit, that is smaller than 10-15 (Bayo et al. 2008). The errors in the temperature and gravity values calculated by the SED analyses are $\Delta T = 125$ K and $\Delta \log g = 0.25$ respectively. The results of the SED analyses are given in corresponding subsections while the fits are displayed in Figure 3.

Orbital periods of the systems were determined by calculating averages of the differences between two consecutive minima times of the same type. Frequency analyses using `Period04` software (Lenz & Breger 2005) were also applied to the light curves to confirm the calculated orbital period values. The calculated times of minima (Table 1) were also used for a period analysis with the linear variation assumption, and variations in orbital period ΔP and time of minimum light ΔT_0 were derived utilizing the equation $O - C = \Delta T_0 + \Delta P \cdot E$, with the cycle number E. The standard errors (SEs) for the orbital periods were derived by using the equation containing standard deviation (σ) and the number of derived period values (N), $SE = \sigma/\sqrt{N}$. The calculated values are given in the following subsections as well as Table 2.

The analyses were applied by using PHOEBE (Prša & Zwitter 2005) which analyzes the input light curve by via the Wilson–Devinney method (Wilson & Devinney 1971). The inclination i, temperature of the secondary component T_2, mass ratio q, surface potential values of the primary component Ω_1 and luminosity of the primary component L_1 were adjustable

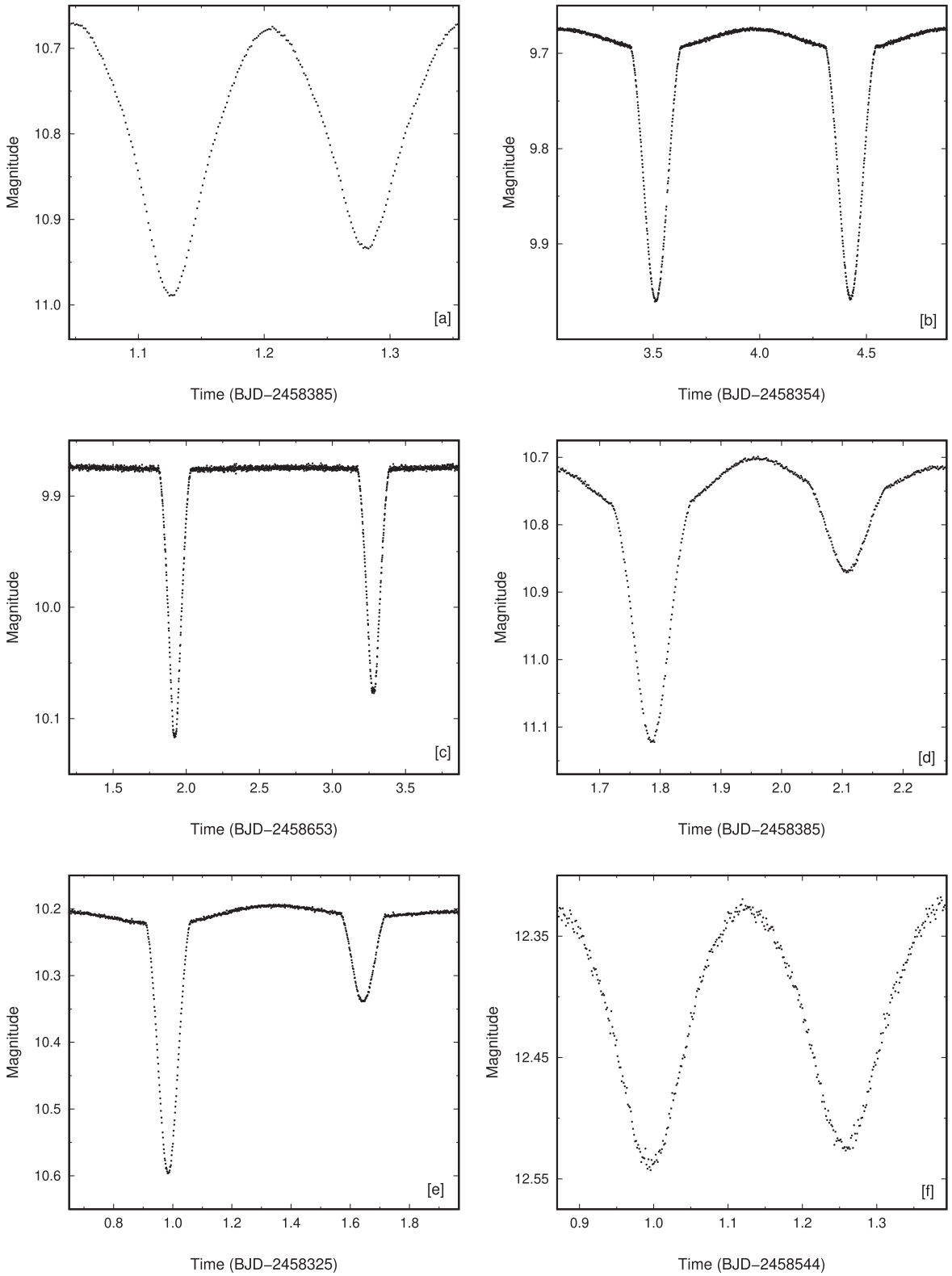

Figure 1. TESS light curve in the time interval equaling one orbital period for CD-54942 (a), CD-58791 (b), CD-621257 (c), TYC 8508-1413-1 (d), TYC 9356-355-1 (e) and UCAC4 136-007295 (f).

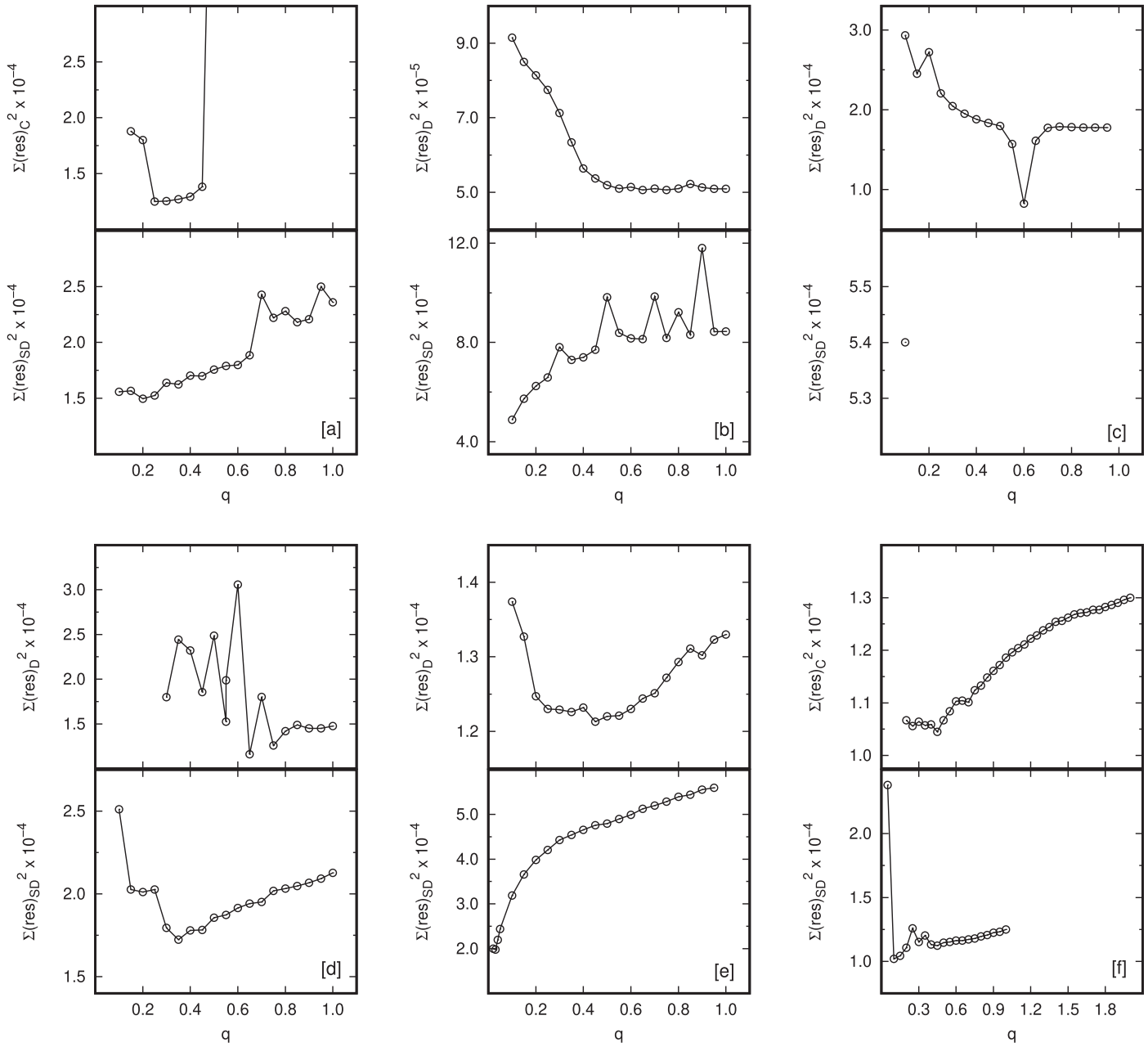

Figure 2. Results of the q-search for CD-54942 (a), CD-58791 (b), CD-621257 (c), TYC 8508-1413-1 (d), TYC 9356-355-1 (e) and UCAC4 136-007295 (f). The sub-indices C, D and SD indicate contact, detached and semidetached morphologies, respectively. Note that the procedure outputted unphysical results for CD-621257 under the semidetached assumption in cases other than the initial value.

parameters in the solutions. Ω_2 was also set as adjustable in the analyses with detached approximation. The albedos (A_1, A_2) were adopted from Ruciński (1969) and the gravity darkening coefficients (g_1, g_2) for the systems were taken from von Zeipel (1924) and Lucy (1967) by taking account of the granulation boundary at about F0 spectral type (Gray & Nagel 1989). Logarithmic limb darkening coefficients (x_1 and x_2) were derived from Claret (2017) based on the initial temperatures of the components. The light curve data covering more than 50,000 data points were reduced to 50,000, the input limit of the software, during the solution.

3.1. CD-54942

The analysis was applied to 50,000 data points which were binned from originally 59,124. The orbital period was set to 0.309691 days, the value derived by using the previously

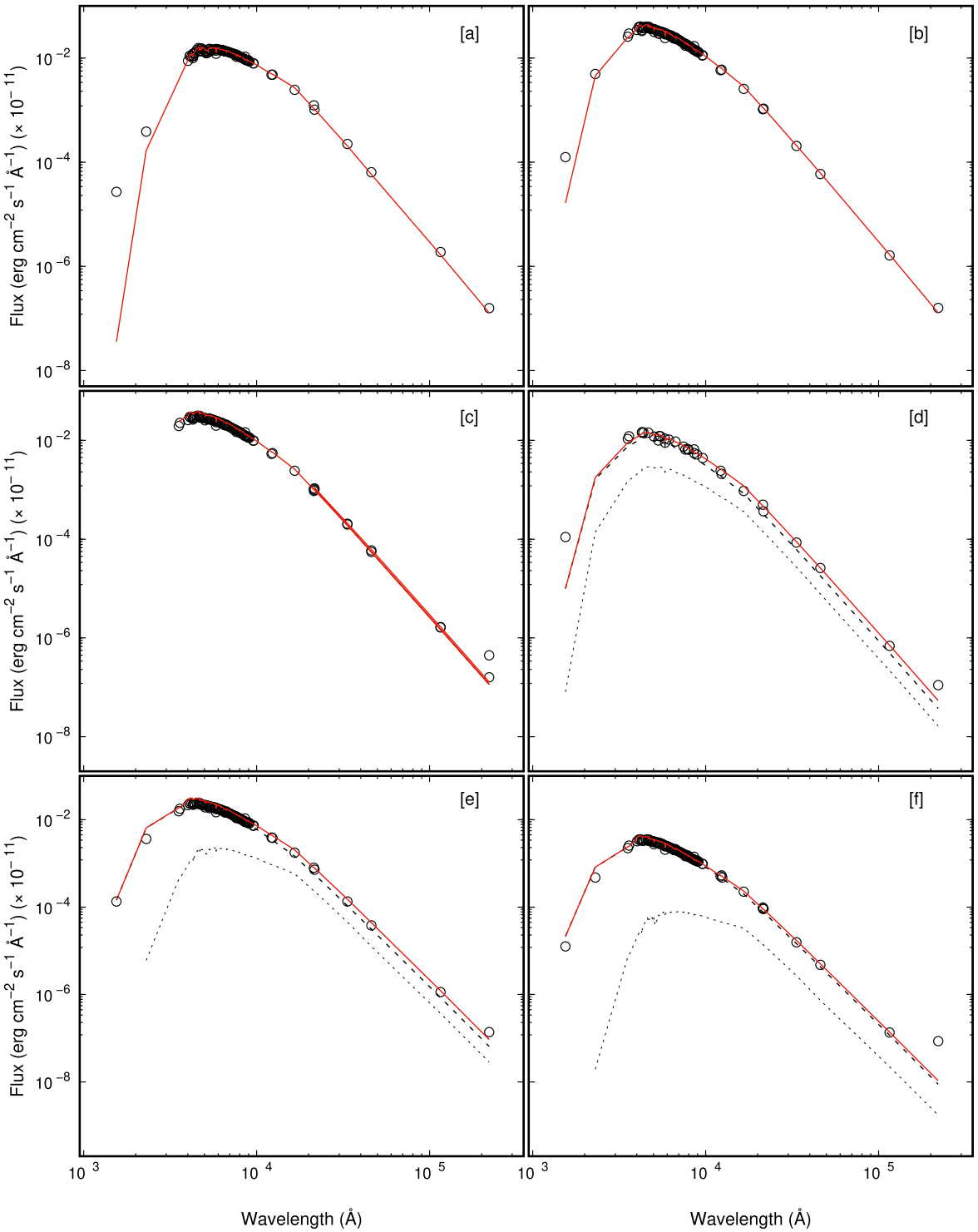

Figure 3. SED fits applied to the available photometric data for CD-54942 (a), CD-58791 (b), CD-621257 (c), TYC 8508-1413-1 (d), TYC 9356-355-1 (e) and UCAC4 136-007295 (f). The red lines refer to the model fits. The dashed and dotted lines in (d), (e) and (f) represent the best model fits for the hotter and cooler components, respectively.

discussed method. Binary fit in the SED analysis resulted in the effective temperatures of the two components as 7250 and 5000 K. However, the first one is quite large compared to the values 5502 K (Steinmetz et al. 2020), 5244 K (Gaia Collaboration et al. 2016, 2022) and 5241 K (Stassun et al. 2019) given in the literature. Therefore, we applied a chi-square

Table 2
Results of the Light Curve Analyses

Parameter	CD-54942	CD-58791	CD-621257
T_0 (BJD)	1435.365982(3)	1355.68657(2)	1654.92067(2)
P (days)	0.309691(4)	1.82630(2)	2.71459(4)
i (°)	66.81(2)	77.922(4)	83.41(1)
q	0.237(1)	0.789(1)	0.608(1)
T_1 (K)	5250(125)	6500(125)	6500(125)
T_2 (K)	4963(21)	6448(10)	6273(33)
Ω_1	2.293(1)	5.022(2)	6.630(6)
Ω_2	Ω_1	4.896(2)	7.90(1)
$L_1/(L_1+L_2)$	0.832(1)	0.5701(4)	0.804(1)
r_1	0.5164(6)	0.2381(7)	0.166(2)
r_2	0.271(3)	0.2097(9)	0.091(4)
$x_1,\ x_2$	0.646, 0.659	0.558, 0.558	0.568, 0.581
	TYC 8508	TYC 9356	UCAC4 136
T_0 (BJD)	1386.143736(7)	1325.984991(7)	1544.00685(2)
P (days)	0.641 91(3)	1.31699(3)	0.52391(8)
i (°)	69.86(2)	79.67(3)	67.46(3)
q	0.580(1)	0.517(1)	0.102(1)
T_1 (K)	6500(125)	7000(125)	7000(125)
T_2 (K)	5058(36)	5548(21)	6682(51)
Ω_1	3.848(6)	5.244(3)	1.956(1)
Ω_2	$\Omega_{cr}=3.027$	4.137(3)	Ω_1
$L_1/(L_1+L_2)$	0.743(1)	0.796(1)	0.905(2)
r_1	0.311(3)	0.212(1)	0.583(1)
r_2	0.331(1)	0.179(2)	0.210(6)
$x_1,\ x_2$	0.570, 0.617	0.547, 0.670	0.548, 0.601

Note. TYC 8508, TYC 9356 and UCAC4 136 refer to TYC 8508-1413-1, TYC 9356-355-1 and UCAC4 136-007295, respectively. The standard deviations, 3σ for the last digits of light parameters, are given in parentheses. The errors in the effective temperature, T_1, are from the corresponding SED analyses. See text for the error determination for orbital period values, P.

fit to determine a more realistic temperature and derived the value of 5250 K. The $\log g$ was also found to be 4.5. The distance is 157.4(3) based on the Gaia Data Release 3 (DR3) parallax (Gaia Collaboration et al. 2016, 2022) and the extinction is $0\overset{m}{.}0342$, derived by using the Galactic Dust Reddening and Extinction interface of NASA/IPAC Infrared Science Archive.[2] The components are assumed to be in solar abundance. The V_{gfb} of the resulting fit is 0.704, which agrees with the criterion for a good fit. The result is shown in Figure 3.

The effective temperature of the hotter component is adjusted to 5250 K during the light curve solution following the SED analysis. The light curve solution was conducted in contact and semidetached approximations with the initial value of the mass ratios of 0.25 and 0.2 considering the q-search. A significantly better fit with smaller squared residuals was achieved with the contact approach. Additionally, a spotted area on the cooler components was hypothesized to fit the difference between the maxima of the light curve. The parameters of the spot are found to be $\beta=45°$, $\lambda=90°$, $r=25°$ and $t=0.9$, where β, λ, r and t are co-latitude, longitude, fractional radius and temperature factor, respectively. The results of the analysis are listed in Table 2 while the agreement with the final fit to the observations is affirmed in Figure 4. We conclude that the target can be considered as a contact binary system.

[2] https://irsa.ipac.caltech.edu/applications/DUST/

3.2. CD-58791

The SED analysis for the system resulted in two temperature values, 7750 and 6500 K, using the binary fit approach. However, the former temperature is contrary to the values given by Gaia Collaboration et al. (2016, 2022); Stassun et al. (2019) and Kordopatis et al. (2013) which are between 6000 and 6600 K. Therefore, we decided to analyze the SED by using the chi-square fit option. The result indicated that $\log g=4.0$ with the temperature value of 6500 K which we set as the temperature of the primary component in our light curve analysis. The extinction was set to $0\overset{m}{.}0736$ and the distance was taken as 416(2) pc following Gaia Collaboration et al. (2016, 2022). The V_{gfb} of the solution, 0.81, corresponds to a good fit. The SED fit is plotted in Figure 3. The orbital period of the system, on the other hand, was calculated as 1.82630 by following the method described earlier.

The light curve analyses were conducted on 44,540 data points in two morphologies, detached and semidetached, individually. Although the semidetached configuration shows relatively small squared residuals in the minimum of the q-search curve, the detached configuration fits the observations better in the light curve analysis. The reason may arise from the fact that the mass ratio is not sensitive to the light curve in detached configuration and weakly depends on it in semidetached binaries showing partial eclipses (Terrell & Wilson 2005). The results are shown in Table 2 as well as in Figure 4. Considering the above-mentioned arguments, we conclude that the system is a detached binary.

3.3. CD-621257

The temperature of the primary components was derived in the same method that was described in previous subsections. The chi-square fit resulted in $\log g=4.5$ and $T=6500$ K which agree with the values given by Gaia Collaboration et al. (2016, 2022) and Stassun et al. (2019). The distance of the system was set to 455(7) pc based on the parallax by Gaia Collaboration et al. (2016, 2022), thus, the extinction is $0\overset{m}{.}1629$. The V_{gfb} was derived as 0.577, which quite agrees with the acceptable interval. Furthermore, the orbital period of the system was calculated to be 2.71459 days using the method discussed above.

The light curve of the binary was analyzed by assuming that the system is a detached binary considering not only the q-

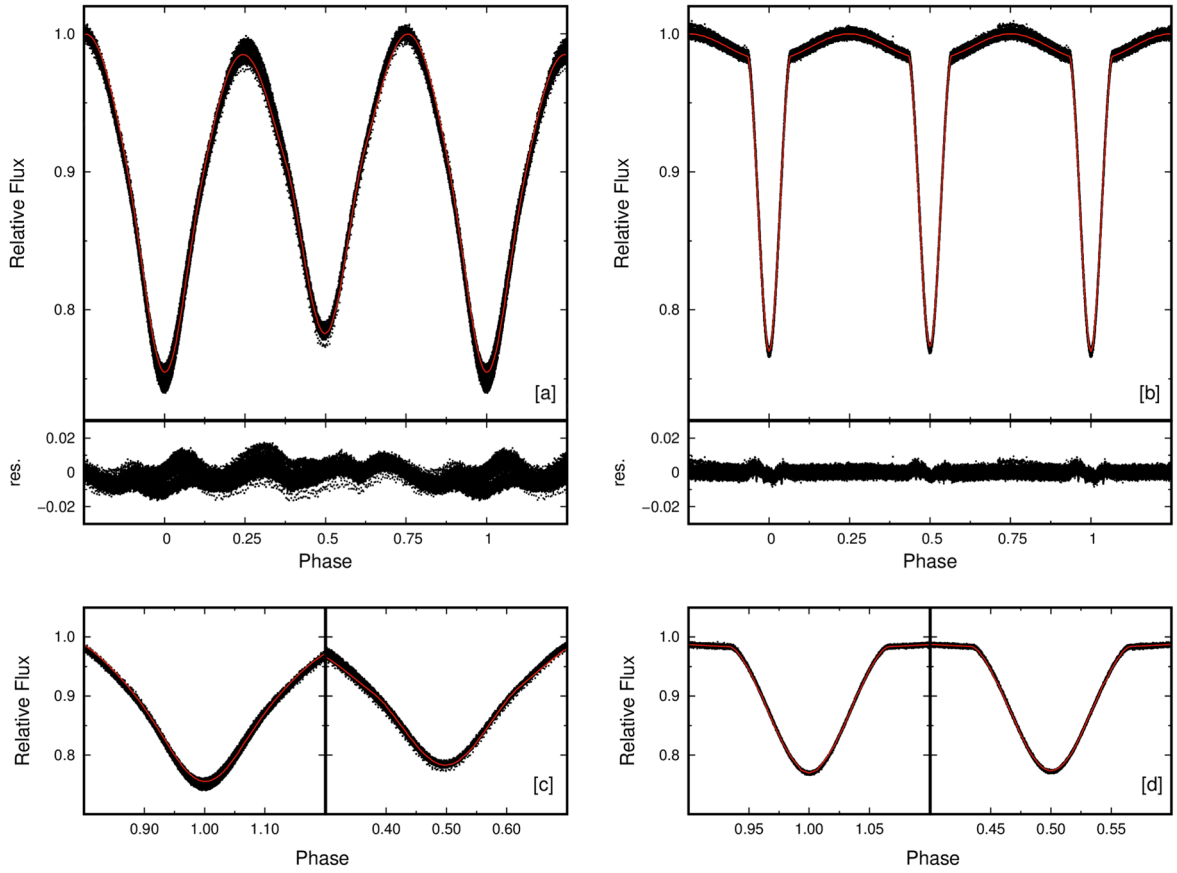

Figure 4. Calculated light curve (red lines) is plotted with the observations and the agreements at the minimum phases are shown for CD-54942 (a), (c) and CD-58791 (b), (d).

search but also the period value and the shape of the light curve. The number of data in the solution was 19,581. The calculated light curve is shown with the observations in Figure 5 while the results are listed in Table 2.

3.4. TYC 8508-1413-1

SED analysis applied to available photometric data by using a binary fit which resulted in $T_1 = 6500$ K, $T_2 = 5750$ K and $\log g_1 = \log g_2 = 4.5$, the values assumed as the initial parameters for the components during the light curve analysis. The V_{gfb} of the fit was calculated as 4.81, smaller than 10–15. The distance of the system was adopted as 374(2) pc (Gaia Collaboration et al. 2016, 2022) which corresponds to an extinction value of $A_V = 0^{\rm m}.04$.

The analysis was applied to 12,399 data points with detached and conventional semidetached approaches individually. Although the residuals of the light curve solution were close in two morphologies, the fillout factor for the secondary component was calculated to be 99%, using the equation $1 - [(\Omega_2 - \Omega_{\rm cr})/\Omega_{\rm cr}]$ in the detached approximation, where $\Omega_{\rm cr}$ signifies the critical potential value for the corresponding mass ratio. In addition, the K spectral type of the secondary is typical for the secondaries of Algol-type binaries. Therefore, the semidetached configuration was supposed to be a more reliable morphology of the system. The initial mass ratio was set to 0.35 and the orbital period was taken as 0.64191 day during the solution. The albedo of the secondary component was set as a free parameter for the first couple of runs in order to achieve a better fit around the secondary minimum. A hot spotted area on the primary component, which may have been the result of mass transfer from the secondary, was also included in the solution to fit the difference between levels at maximum phases. The spot parameters are $\beta = 90°$, $\lambda = 240°$, $r = 15°$ and $t = 1.05$. The resulting parameters are listed in Table 2. The calculated and observational light curves are displayed in Figure 5.

3.5. TYC 9356-355-1

A binary fit with $V_{gfb} = 0.35$ in the SED analysis corresponded to the temperature of the primary and secondary

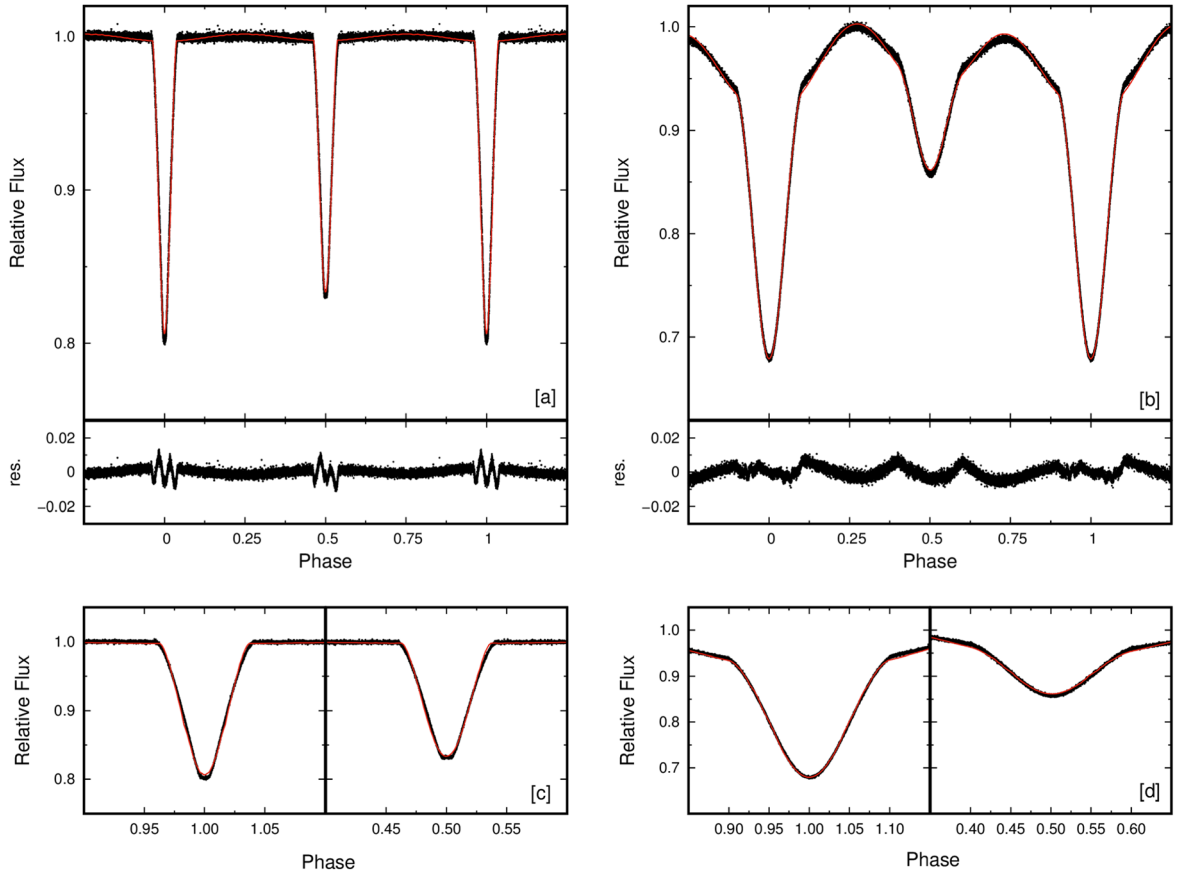

Figure 5. Same as Figure 4, but for CD-621257 (a), (c) and TYC 8508-1413-1 (b), (d).

components being $T_1 = 7000$ K and $T_2 = 4750$ K respectively while the $\log g$ values were found to be 4.5 for both of the components. The extinction was adopted to $0^{\rm m}.2026$ and the distance of the system is 320(4) pc (Gaia Collaboration et al. 2016, 2022). The orbital period was calculated as 1.31699 by using the method mentioned earlier in the text.

The orbital period value, the result of the q-search and the shape of the light curve led us to analyze the light curve, which covers 37,859 data points in detached mode and, therefore, the initial value for the mass ratio was set to 0.5. The calculated light curve is plotted with observations in Figure 6 and the light parameters found by the solution are given in Table 2.

3.6. UCAC4 136-007295

The temperatures and gravities of the components were calculated as $T_1 = 7000$ K, $T_2 = 4250$ K and $\log g_1 = \log g_2 = 4.0$ during the SED analysis respectively; the former is relatively close to the value given by Sharma et al. (2018), 6529 K, in their catalog. The distance of the system is 1295(68) pc (Gaia Collaboration et al. 2016, 2022), and the extinction in that direction is $A_V = 0^{\rm m}.1195$, which was yielded using the same method given above. The goodness of fit for the solution, $V_{gfb} = 0.218$, corresponds to a good fit.

We analyzed the light curve in two morphological assumptions; semidetached (with a secondary filling its Roche lobe) and contact. The semidetached analysis resulted in a warning that the primary component exceeds its corresponding Roche lobe. Thereby, the solution was conducted using 41,110 light curve data with an approach that the binary is a contact system. The calculated light curve is plotted with the observations in Figure 6 and the results are listed in Table 2.

4. Conclusion

We presented a comprehensive study on the binary properties of six eclipsing binary systems. The absolute parameters (Table 3) are derived based on the light parameters by using the `AbsParEB` program (Liakos & Niarchos 2015). It is worth emphasizing that the errors in Tables 2 and 3 are unphysical since the uncertainties in the Wilson–Devinney method are underestimated. Furthermore, the relatively poor fit caused deviations from the observations around the minimum phases of some systems. The maximum value of the amplitude of

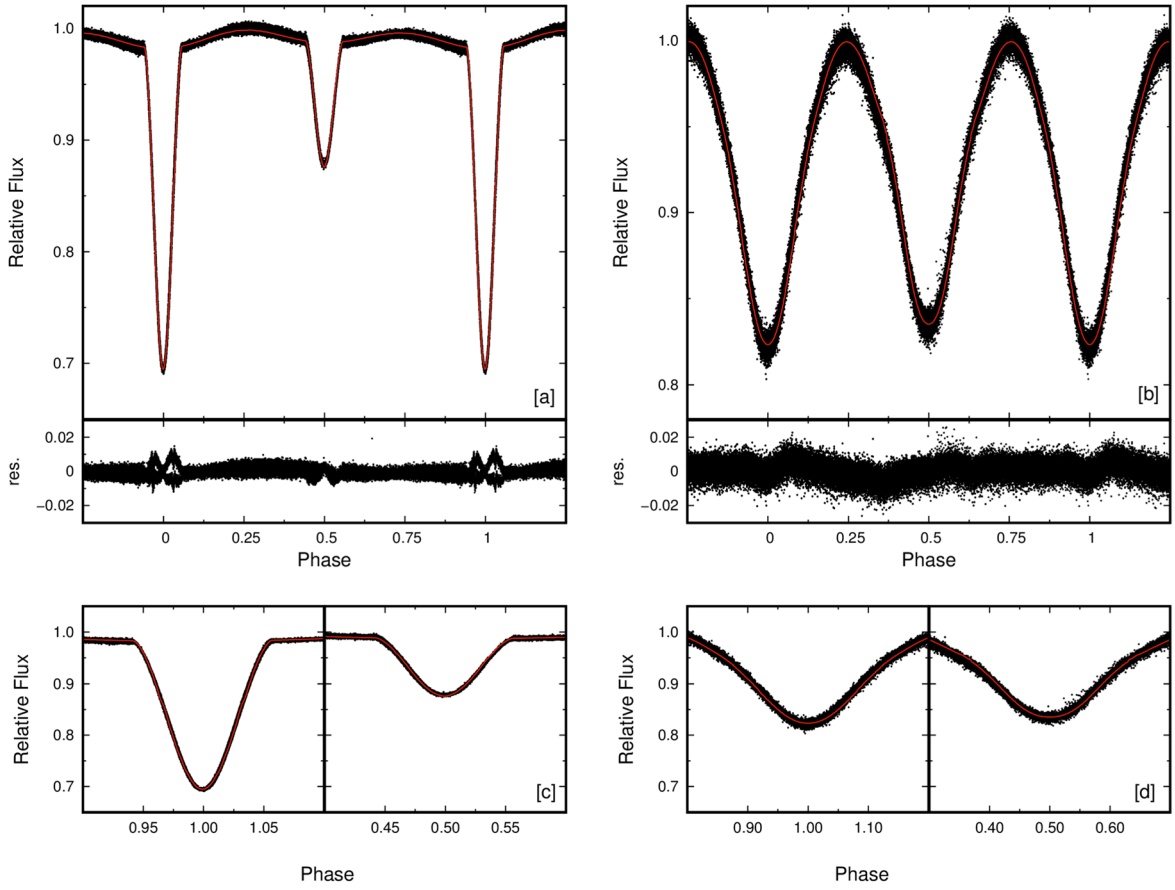

Figure 6. Same as Figure 4, but for TYC 9356-355-1 (a, c) and UCAC4 136-007295 (b, d).

Table 3
Absolute Parameters of the Systems

Parameter	CD-54942	CD-58791	CD-621257
M_1 ($M_\odot$)	0.8	1.5	2.1
M_2 ($M_\odot$)	0.190(1)	1.183(2)	1.277(2)
R_1 ($R_\odot$)	1.015(2)	2.13(1)	2.09(9)
R_2 ($R_\odot$)	0.53(1)	1.87(2)	1.1(3)
L_1 ($L_\odot$)	0.701(2)	7.2(1)	6.9(6)
L_2 ($L_\odot$)	0.154(7)	5.4(1)	1.8(9)
a ($R_\odot$)	1.965(2)	8.943(4)	12.57(1)
	TYC 8508	TYC 9356	UCAC4 136
M_1 ($M_\odot$)	1.3	1.5	1.6
M_2 ($M_\odot$)	0.754(1)	0.776(2)	0.163(2)
R_1 ($R_\odot$)	1.27(2)	1.44(2)	1.972(4)
R_2 ($R_\odot$)	1.35(1)	1.22(4)	0.71(5)
L_1 ($L_\odot$)	2.57(9)	4.4(1)	8.36(3)
L_2 ($L_\odot$)	1.07(1)	1.26(9)	0.9(1)
a ($R_\odot$)	4.074(2)	6.807(4)	3.382(3)

Note. TYC 8508, TYC 9356 and UCAC4 136 refer to TYC 8508-1413-1, TYC 9356-355-1 and UCAC4 136-007295, respectively. The standard errors are given in parentheses for the last digits.

deviation was calculated as $0\overset{m}{.}02$ for CD-58791 and TYC 8508-1413-1, while it was $0\overset{m}{.}03$ for CD-621257 and TYC 9356-355-1. The masses of the primary components of contact and semidetached systems (CD-54942, TYC 8508-1413-1 and UCAC4 136-007295) were estimated among 204 930 binary star models created by using the Binary Star Evolution code by Hurley et al. (2002, 2013) by setting the initial parameters of the orbital period between 0.5 d and 7 d, the eccentricity between 0 and 0.5, the mass of the primary component, M_1, between 0.5 $M_\odot$ and 5.0 $M_\odot$, and the mass of the secondary component between 0.1 and M_1. The masses for the primaries of the detached systems (CD-58791, CD-621257 and TYC 9356-355-1) were calculated from the stellar tracks of Bertelli et al. (2009) according to their log g and effective temperature values. The stars are assumed to be in solar abundance during calculations.

The fill-out factor, which indicates the degree of contact between components, for the contact binaries CD-54942 and UCAC4 136-007295 was found to be 0.19 and 0.42 by using the equation $f = (\Omega_i - \Omega)/(\Omega_i - \Omega_o)$ (Kallrath & Milone 2009), where Ω_i and Ω_o are the inner and outer Lagrangian

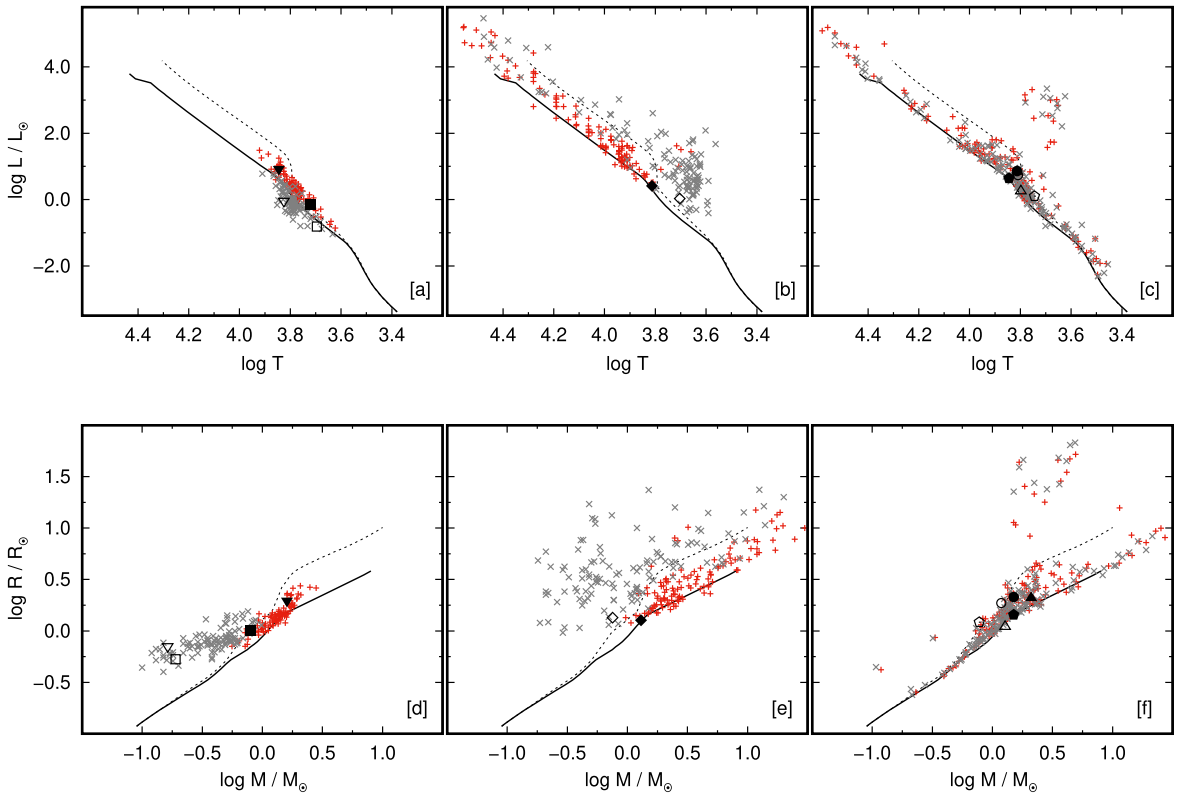

Figure 7. The upper panel shows the Hertzsprung–Russell diagrams while the lower panel indicates the mass–radius planes for contact (a), (d), semidetached (b), (e) and detached (c), (f) binary systems. Plus and cross symbols signify the primaries and secondaries of well-known systems with the corresponding morphology respectively. Full and open signs refer to primary and secondary components respectively. Squares, circles, triangles, diamonds, pentagons and upside-down triangles correspond to CD-54942, CD-58791, CD-621257, TYC 8508-1413-1, TYC 9356-355-1 and UCAC4 136-007295, respectively. Note that the location of the primary components of CD-58791 and CD-621257 overlap on the Hertzsprung–Russell diagram (c). The data for Zero Age Main Sequence (ZAMS, thick solid line) and Terminal Age Main Sequence (TAMS, dashed line) are taken from Bressan et al. (2012) with $Y = 0.267$ and $Z = 0.01$ abundance.

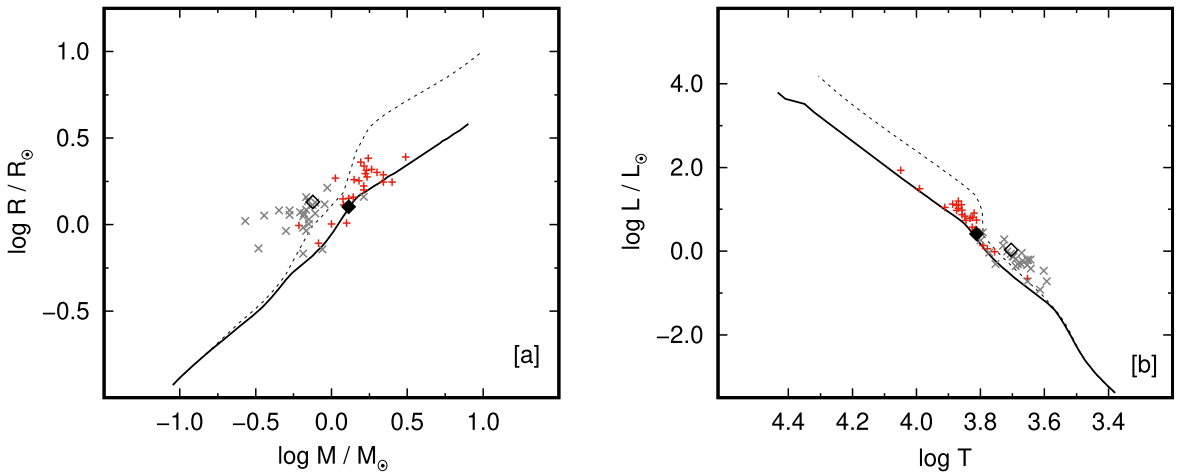

Figure 8. Same as Figure 7, but for TYC 8508-1413-1 and the known near-contact binaries.

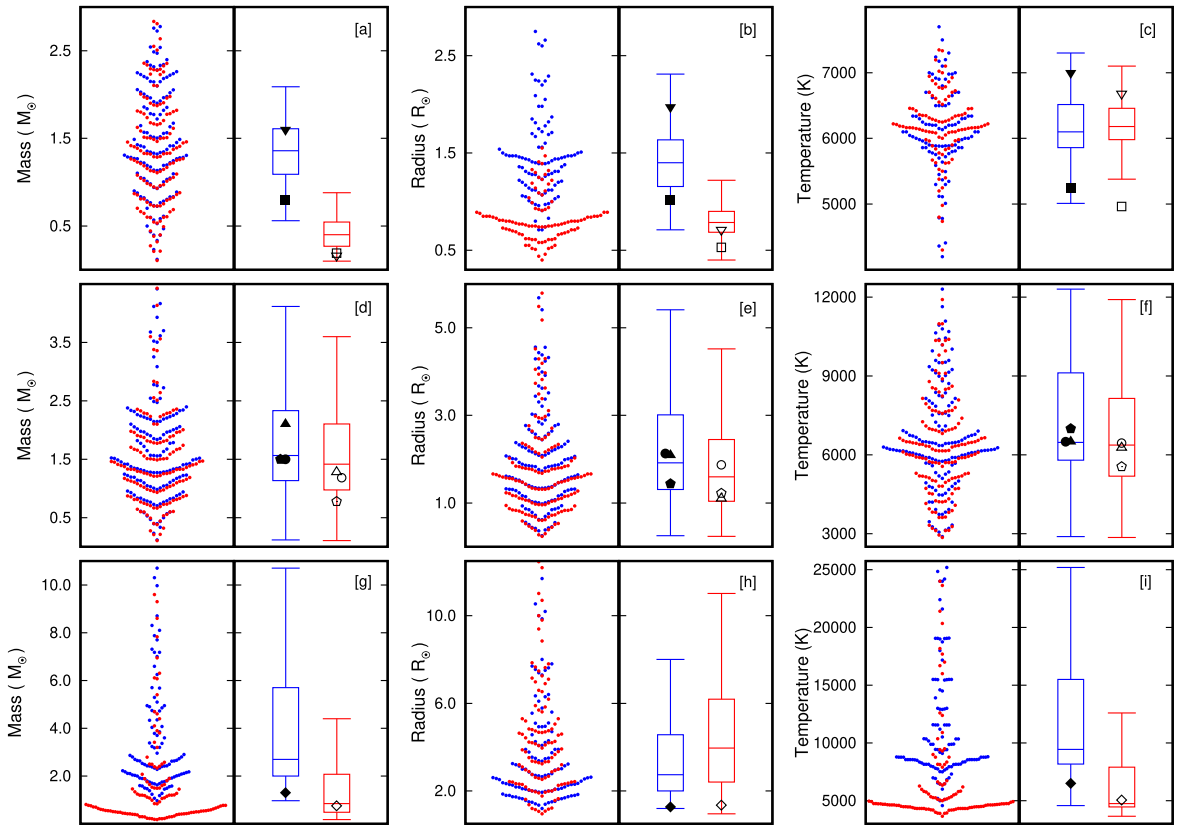

Figure 9. Mass, radius and temperature distributions (left panels) and corresponding box plots (right panels) for primary (blue) and secondary (red) components of known contact (a)–(c), detached (d)–(f) and semidetached (g)–(i) binary systems. The other symbols are the same as those displayed in Figure 7. Some extreme values are excluded in plots, however, boxes are calculated using all available data.

Table 4
Parameters of Box Plot Calculated by Using Data from 100 Contact (Yıldız & Doğan 2013), 162 Detached (Southworth 2015) and 119 Semidetached (Malkov 2020) Binaries

	$Q1$	$Q2$	$Q3$	min.	max.	IQR
Contact						
M_1 ($M_\odot$)	1.09	1.36	1.61	0.56	2.09	0.52
M_2 ($M_\odot$)	0.27	0.40	0.55	0.10	0.88	0.28
R_1 ($R_\odot$)	1.16	1.40	1.58	0.71	2.20	0.43
R_2 ($R_\odot$)	0.69	0.78	0.89	0.40	1.19	0.21
T_1 (K)	5860	6100	6500	5012	7300	640
T_2 (K)	5982	6180	6453	5380	7102	472
Detached						
M_1 ($M_\odot$)	1.13	1.56	2.33	0.12	4.12	1.19
M_2 ($M_\odot$)	0.97	1.41	2.10	0.11	3.60	1.13
R_1 ($R_\odot$)	1.31	1.92	2.98	0.25	5.41	1.67
R_2 ($R_\odot$)	1.04	1.59	2.43	0.24	4.29	1.38
T_1 (K)	5798	6471	9094	2892	12,303	3296
T_2 (K)	5191	6375	8133	2851	11,912	2942
Semidetached						
M_1 ($M_\odot$)	2.01	2.71	5.69	0.97	10.70	3.68
M_2 ($M_\odot$)	0.48	0.88	2.03	0.18	4.10	1.55
R_1 ($R_\odot$)	2.00	2.74	4.50	1.20	8.00	2.50
R_2 ($R_\odot$)	2.41	4.01	6.12	0.96	11.02	3.70
T_1 (K)	8283	9660	15 498	4570	25,200	7215
T_2 (K)	4465	4803	7615	3650	10,900	3150

Note. $Q1$, $Q2$, $Q3$ and IQR refer to lower quartile, median, upper quartile and interquartile range values respectively.

potentials. The filling factor ($f = r/r_L$) for the primary component of the semidetached system TYC 8508-1413-1, on the other hand, was calculated by using the relation $r_L = 0.49q^{\frac{2}{3}}/[0.6q^{\frac{2}{3}} + \ln(1 + q^{\frac{1}{3}})]$ given by Eggleton (1983), where r_L is the Roche lobe radius. The f was found to be 0.93 which indicates that the component is close to its Roche lobe and the binary can be considered as a V1010 Oph type near-contact binary group based on the classification

of Shaw (1994). The difference between the maximums of the light curve also supports this classification.

The systems were compared to the known binaries with the same morphological type in Figure 7. The plots confirm that the components of the systems are in good agreement with 100 contact (Yıldız & Doğan 2013), 162 detached (Southworth 2015) and 119 semidetached (Malkov 2020) binary systems. We also compare TYC 8508-1413-1 to 26 known near-contact systems given by Yakut & Eggleton (2005) in Figure 8 in order to check its possible near-contact candidacy remarked in the previous paragraph. The components of the target are in accordance with the other near-contact binaries. A further statistical comparison was made through the known systems' mass, radius and temperature distributions similar to those done by Ulaş & Ulusoy (2023). Figure 9 illustrates the distributions and the box plots calculated by using the data of corresponding stellar parameters. The masses, radii and temperatures of our target systems are well inside the minimum and maximum values although the secondary component of CD-54 942 seems to be cooler than most of its cousins. The parameters of the box plots are given in Table 4.

We concluded that TYC 8508-1413-1 is a semidetached system with a high probability of being a V1010 Oph type near-contact system. CD-54942 and UCAC4 136-007295 are contact binaries and CD-58791, CD-621257 and TYC 9356-355-1 are detached systems. Spectroscopic studies in combination with our results may lead to determining the characteristics of the systems more precisely.

Acknowledgments

This work was supported by Çanakkale Onsekiz Mart University, The Scientific Research Coordination Unit, Project number: 2022-FBA-3851. The numerical calculations reported in this paper were partially performed at TUBITAK ULAKBIM, High Performance and Grid Computing Center (TRUBA resources). This paper includes data collected by the TESS mission. Funding for the TESS mission is provided by NASA's Science Mission Directorate. Some/all of the data presented in this paper were obtained from the Mikulski Archive for Space Telescopes (MAST). STScI is operated by the Association of Universities for Research in Astronomy, Inc., under NASA contract NAS5-26555. Support for MAST for non-HST data is provided by the NASA Office of Space Science via grant NNX13AC07G and by other grants and contracts. This research has made use of the NASA/IPAC Infrared Science Archive, which is operated by the Jet Propulsion Laboratory, California Institute of Technology, under contract with the National Aeronautics and Space Administration. This publication makes use of VOSA, developed under the Spanish Virtual Observatory project supported by the Spanish MINECO through grant AyA2017-84089. VOSA has been partially updated by using funding from the European Union's Horizon 2020 Research and Innovation Programme, under Grant Agreement No. 776403 (EXOPLANETS-A). This research has made use of NASA's Astrophysics Data System. This research has made use of the VizieR catalog access tool, CDS, Strasbourg, France. This work has made use of data from the European Space Agency (ESA) mission Gaia (https://www.cosmos.esa.int/gaia), processed by the Gaia Data Processing and Analysis Consortium (DPAC, https://www.cosmos.esa.int/web/gaia/dpac/consortium). Funding for the DPAC has been provided by national institutions, in particular the institutions participating in the Gaia Multilateral Agreement.

ORCID iDs

Burak Ulaş https://orcid.org/0000-0002-4624-3847

References

Bayo, A., Rodrigo, C., Barrado Y Navascués, D., et al. 2008, A&A, 492, 277
Bertelli, G., Nasi, E., Girardi, L., & Marigo, P. 2009, A&A, 508, 355
Borucki, W. J., Koch, D., Basri, G., et al. 2010, Sci, 327, 977
Bressan, A., Marigo, P., Girardi, L., et al. 2012, MNRAS, 427, 127
Claret, A. 2017, A&A, 600, A30
Eggleton, P. P. 1983, ApJ, 268, 368
Gaia Collaboration, Brown, A. G. A., Vallenari, A., et al. 2018, A&A, 616, A1
Gaia Collaboration, Prusti, T., de Bruijne, J. H. J., et al. 2016, A&A, 595, A1
Gaia Collaboration, Vallenari, A., Brown, A. G. A., et al. 2022, arXiv:2208.00211
Gray, D. F., & Nagel, T. 1989, ApJ, 341, 421
Hurley, J. R., Tout, C. A., & Pols, O. R. 2002, MNRAS, 329, 897
Hurley, J. R., Tout, C. A., & Pols, O. R. 2013, BSE: Binary Star Evolution, Astrophysics Source Code Library, ascl:1303.014
Kallrath, J., & Milone, E. F. 2009, Eclipsing Binary Stars: Modeling and Analysis (Berlin: Springer)
Kirk, B., Conroy, K., Prša, A., et al. 2016, AJ, 151, 68
Kordopatis, G., Gilmore, G., Steinmetz, M., et al. 2013, AJ, 146, 134
Kunder, A., Kordopatis, G., Steinmetz, M., et al. 2017, AJ, 153, 75
Kurucz, R. L. 1979, ApJS, 40, 1
Kwee, K. K., & van Woerden, H. 1956, BAIN, 12, 327
Lenz, P., & Breger, M. 2005, CoAst, 146, 53
Liakos, A., & Niarchos, P. 2015, in ASP Conf. Ser. 496, Living Together: Planets, Host Stars and Binaries, ed. S. M. Rucinski, G. Torres, & M. Zejda (San Francisco, CA: ASP), 195
Lucy, L. B. 1967, ZAp, 65, 89
Malkov, O. Y. 2020, MNRAS, 491, 5489
Ochsenbein, F., Bauer, P., & Marcout, J. 2000, A&As, 143, 23
Prša, A., Kochoska, A., Conroy, K. E., et al. 2022, ApJS, 258, 16
Prša, A., & Zwitter, T. 2005, ApJ, 628, 426
Ricker, G. R., Winn, J. N., Vanderspek, R., et al. 2015, JATIS, 1, 014003
Ruciński, S. M. 1969, AcA, 19, 245
Sharma, S., Stello, D., Buder, S., et al. 2018, MNRAS, 473, 2004
Shaw, J. S. 1994, MmSAI, 65, 95
Southworth, J. 2015, in ASP Conf. Ser. 496, Living Together: Planets, Host Stars and Binaries, ed. S. M. Rucinski, G. Torres, & M. Zejda (San Francisco, CA: ASP), 164
Stassun, K. G., Oelkers, R. J., Paegert, M., et al. 2019, AJ, 158, 138
Steinmetz, M., Guiglion, G., McMillan, P. J., et al. 2020, AJ, 160, 83
Terrell, D., & Wilson, R. E. 2005, Ap&SS, 296, 221
Ulaş, B., & Ulusoy, C. 2023, MNRAS, 518, 4180
von Zeipel, H. 1924, MNRAS, 84, 665
Wilson, R. E., & Devinney, E. J. 1971, ApJ, 166, 605
Wilson, R. E., Devinney, E. J., & Van Hamme, W. 2020, WD: Wilson–Devinney Binary Star Modeling, Astrophysics Source Code Library
Yakut, K., & Eggleton, P. P. 2005, ApJ, 629, 1055
Yıldız, M., & Doğan, T. 2013, MNRAS, 430, 2029